Convection and the Tropics

Peter Bechtold

ECMWF, Shinfield Park, Reading, UK
peter.bechtold@ecmwf.int

1 Heat and momentum balances

Analysing the tropical convection in a forecast system is a huge and difficult task. Due to the small Coriolis force and large Rossby radius of deformation near the Equator as well as fast propagating gravity waves that export the convective heating (Bretherton and Smolarkiewicz, 1989), convection affects a vast variety of space and time scales, from the individual convective cloud to the large-scale convectively coupled waves (e.g. Simmons, 1982; Žagar et al., 2005), the intraseasonal oscillations, and the Monsoon circulations. Furthermore, it is difficult to observe convection as such or all the convective transport processes. It is therefore appropriate to describe convection by measuring the quality of the model in terms of convection and cloud related quantities such as surface precipitation, outgoing longwave radiation (OLR), and observables such as the temperature, moisture and wind fields.

In Figure 1 are depicted the tendencies for temperature and u-momentum from the physics and the dynamics averaged over the tropical belt as obtained from 24 hour forecasts with the ECMWF Integrated Forecast System (IFS). The temperature budget is largely determined by heating of the boundary-layer by surface turbulent fluxes, cooling of the troposphere at a rate of 1-2 K day^{-1} by longwave emission, and this vertical destabilisation is offset by convective heating (mainly through condensation, but also vertical transport), so that the tropical atmosphere is in approximate radiative-convective equilibrium. For momentum there is a fine balance between the dynamics (pressure gradient), turbulent diffusion and convective momentum transport, mainly by shallow convection. It appears from Figure 1 that shallow convection accelerates the near surface easterly winds but slows down the winds in the upper part of the trade-wind boundary-layer. The total tendencies is close to zero when avearged over the tropical belt (black lines in Figure 1), and if not this is indicative for model biases as here e.g. a cold bias at 700 hPa and too strong tropical easterlies near 200 hPa.

Instead of average heating profiles one can extract characteristic deep convective and stratiform profiles by sampling over columns where susbtantial rain occcurs and either of the two categories dominates (Figure 2). The typical deep convetive profile is then a parabolic profile with a maximum around 500 hPa, whereas the stratiform profile exhibits the characteristic heating/cooling dipole. Non-dimensional profiles can be obtained by normalizing with the local precipitation rate. These exhibit a characteristic bottom-heavy structure for deep convection and a clear heating/cooling dipole for

grid-scale precipitation. As these profiles imply very different dynamical responses, it is important for a forecast model to have an optimal partitioning between convective (subgrid-scale) and gridscale precipitation; in the IFS this ratio is about 3/1 in the Tropics.

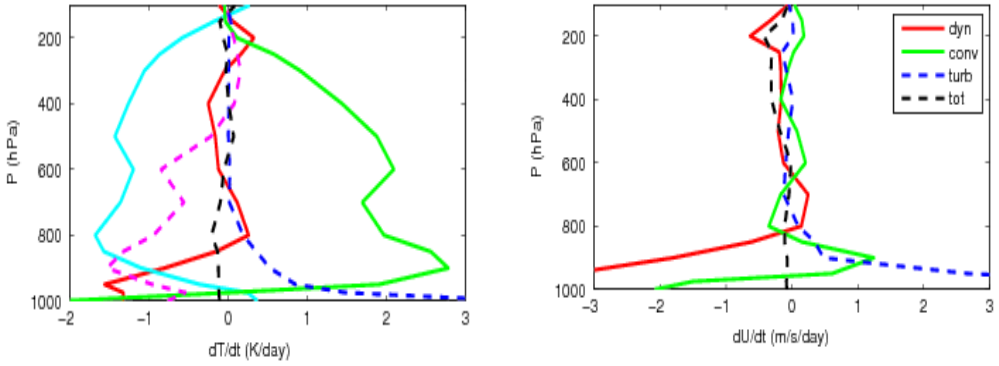

Figure 1: Temperature tendencies (K day^{-1}) and u-wind tendencies (m s^{-1} day^{-1}) from the individual processes: dynamics (red), turbulent diffusion (blue), convection (green), radiation (cyan), and stratiform or grid-scale microphysics (pink). The total model tendencies correspond to dashed black lines.

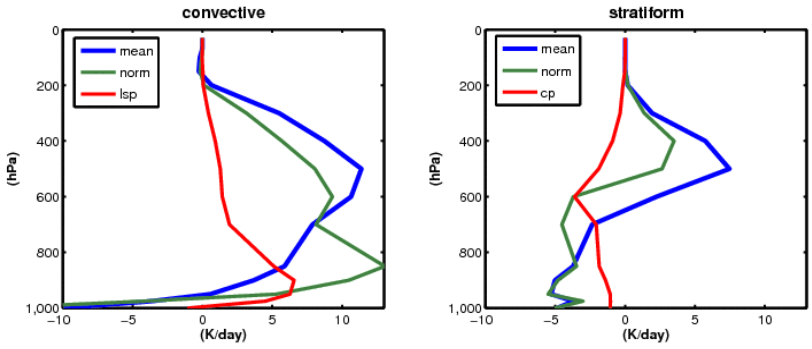

Figure 2: 'Pure' convective (stratiform) heating profiles sampled only over columns where the convective (stratiform) rainfall rate is at least 2 mm day^{-1}, and at least 3 times as large as its stratiform (convective) counterpart: blue lines. Non-dimensional heating profiles are obtained when individual convective (stratiform) columns are normalized by the rain rate at each grid-point: green lines. The red profiles are obtained when the sampling of convective (stratiform) tendencies is done over stratiform (convective) columns.

2 Heating and motions

The change in available potential energy (APE) through thermal generation and its conversion into kinetic energy is best decsribed by the Lorenz energy cycle (Steinheimer et al. 2008)

$$\frac{da}{dt} = N\bar{Q} + \bar{\alpha}\bar{\omega} + \overline{\alpha'\omega'}; \quad N = 1-(p_r / p)^{R/c_p}$$

where the first term on the lhs is the grid-scale generation term with N the Lorenz efficiency factor (depending on a barotropic background pressure pr), and Q the net heating. The conversion into kinetic energy can be defined by grid-scale correlations between the pressure vertical velocity ω and inverse density α, and subgrid-scale contributions the latter being the turbulent and convective buoyancy fluxes. Note that

the concept of convective available potential energy (CAPE) is not included in the concept of APE, but can be indirectly included through the subgrid convective buoyancy flux –the latter is actually more closely linked to the concept of "cloud work function" as postulated as a convecction closure by Arakawa and Schubert (1974).

Generation and conversion rates of APE are illustrated in Figure 3. The main region for generation is the upper-tropical troposphere. However, generation rates from radiation are negative in the Tropics as radiation cools in warm regions, and are only positive in the polar regions where cooling in cold regions takes place. The grid-scale conversion into kinetic energy is also maximum in the upper-tropical troposphere, and negative in the subtropical jet regions, whereas the subgrid conversion rates to which the surface fluxes and the convection are the main contributors, are mostly positive

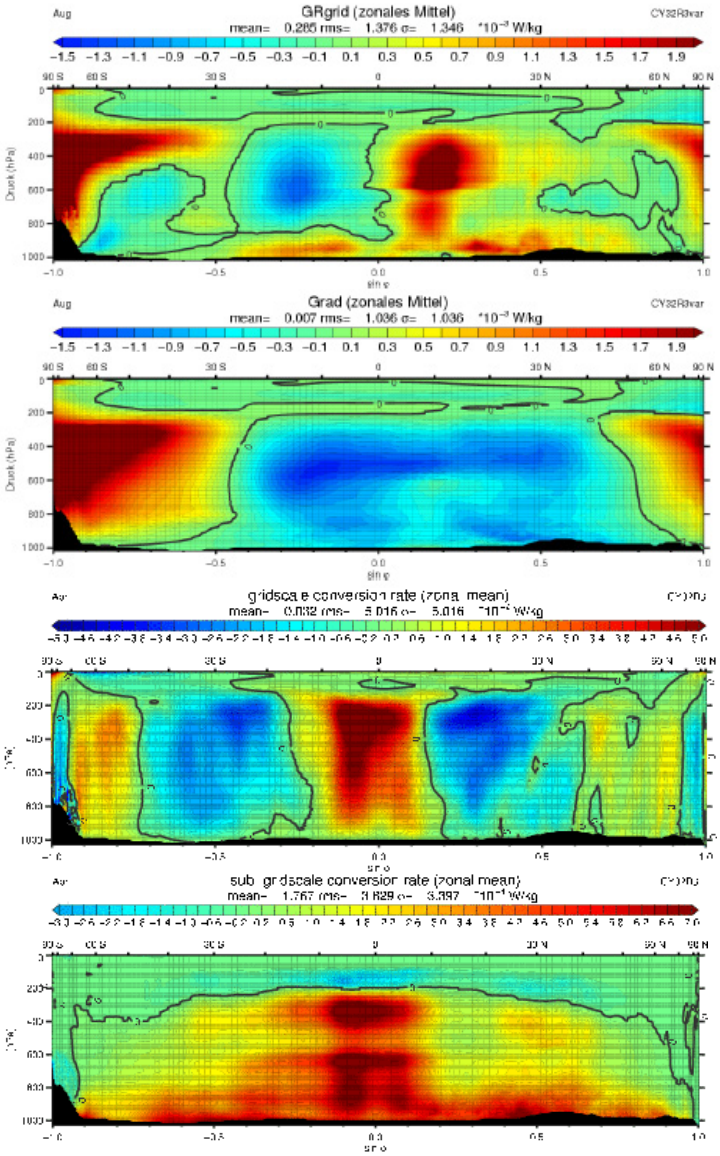

Figure 3. Generation rates during August and conversion ratesduring April of Available Potential Energy: (a) total grid-scale generation rate, (b) generation rate from radiation, (c) total grid-scale conversion rate, and (d) total subgrid-scale conversion rate. The sign convention here is that conversion rates are denoted positive (kinetic energy production) when $-\alpha\omega>0$.

throughout. Nevertheless grid-scale conversion rates are not uniformly positive in the upper-tropical troposphere, but negative in the central and eastern Pacific which also correspond to regions with strongly decaying amplitudes of convectively coupled Kelvin waves and the Madden-Julian Oscillation (MJO) (Madden and Julian, 1971).

3 Convectively coupled waves

The tropical wave motions can be derived from the linearized shallow water system (therefore without the inclusion of a diabatic heating term) as shown back in 1966 by Matsuno. Solutions to these equations for $\psi = u, v, h$ can be described by a wave solution in the x-direction and a solution decaying away from the Equator in the y-direction. The wave field and dispersion relations are given by

$$\psi' = \hat{\psi} H(y) \exp(-y^*/2)\,\mathrm{Re}\{\exp[i(kx-\omega t)]\} \times G(z);\; G(z) = \exp(-z/2H_s)\,\mathrm{Re}\{\exp(imz)\}$$

$$\left(\frac{\omega^2}{c^2} - k^2 - \frac{k}{\omega}\beta\right)\frac{c}{\beta} = 2n+1; n = 0,1,2,..;\; m = \left(\frac{N^2}{c^2} - \frac{1}{4H_s^{\,2}}\right)^{1/2};\; N^2 = \frac{R}{H_s}\frac{d\theta_0}{dz};\; c = \sqrt{gh}$$

where ω is frequency, k, m horizontal and vertical wave number, $\beta = df/dy$, with f the Coriolis parameter c the gravity wave phase speed, N the Brunt Vaisälä frequency, h the equivalent depth, H_s the atmospheric scale height and $H(y)$ Hermite polynomials of order n. Analytical solutions for inertial gravity waves, equatorial Rossby waves and Kelvin waves ($v = 0$) can be obtained from the dispersion relations (see also Bechtold, 2012) for further details. Interestingly the solution for the vertical wave number m implies the horizontal phase speed c, so that if the vertical stability or convective heating become wrong, the vertical wavenumber and the horizontal phase speed will also be wrong. Wave number frequency diagrams for the outgoing longwave radiation

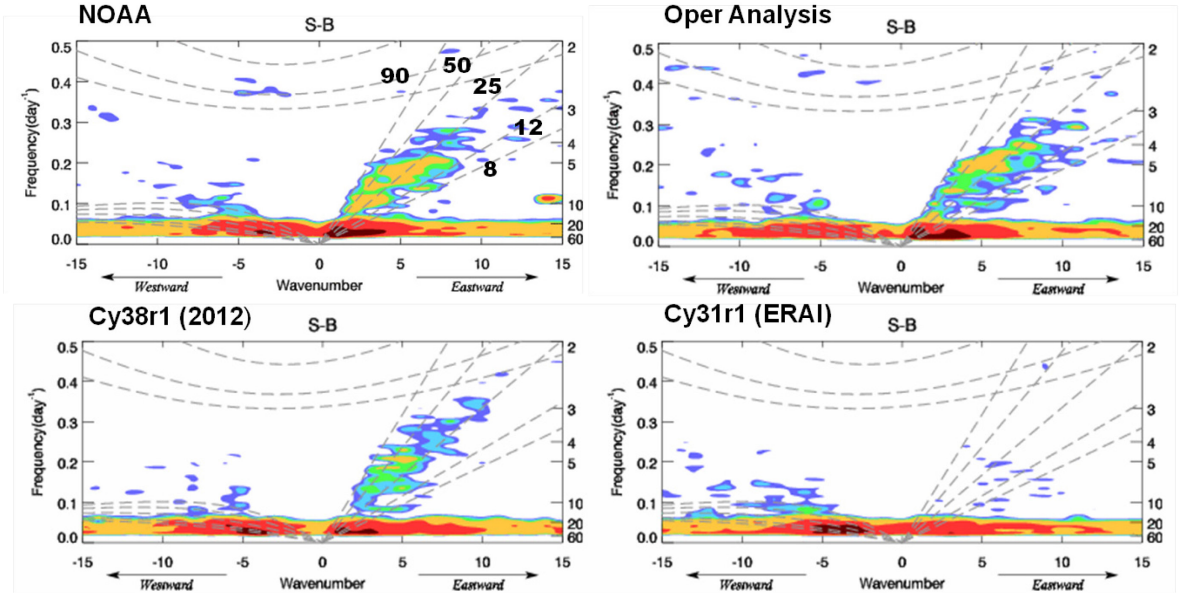

Figure 4. Wavenumber-Frequency spectra of the symmetric component of the OLR from NOAA, the operational analysis 2008-2012, and from an ensemble of 1-year integrations with Cy38R1 and Cy31r1. A background spectrum has been substracted, the theoretical dispersion relations correspond to equivalent depths of 90, 50, 25, 12 and 8 m.

(OLR) are depicted in Figure 4 from both the observations, the analysis, the latest model cycle and the ERA-Interim model cycle in 2006. Indeed, in the observations and analysis the main wave modes become apparent which are also well represented in the latest model cycle, but not in the ERA-Interim (and in all model cycles before 2008) due to wrong convective heating (see Section on the MJO). Finally, note that when waves become convectively coupled they slow down, which is indicated in Figure 4 for the Kelvin waves through different equivalent depths, so that strongly coupled Kelvin waves resemble the MJO mode (spectral maximum in the wavenumber 1-3 and 20-60 day frequency range).

4 The analysis system and short-range forecast errors

Before comparing seasonal forecasts with analysis, it is appropriate to quantify short-range forecast errors and analysis uncertainties. As an overview of the evolution of the high-resolution suite of the IFS in the Tropics over the last decades, time series of tropical ocean precipitation (mm day^{-1}) is shown in Figure 5 from the GPCP2.2 product, as well as from the ERA-Interim and operational day+1 and day+5 forecasts. The GPCP2.2 rain rates are about 3.5 mm day^{-1} compared to the 4.5 mm day^{-1} from the ERA-Interim where the total column water content is strongly constrained by the SSMI microwave retrievals. In 2006 the operational cycle and the ERA-Interim model cycle are equivalent, so are the rain rates, but the large model physics change in 2007 resulted in operational rain rates that with 3.9 mm day^{-1} are now much closer to the GPCP2.2, but there is now a slight increase of precipitation with forecast time due to a moistening tendency in the model. However, we believe that the actual rate over tropical oceans should be somewhere between the GPCP2.2 and operations.

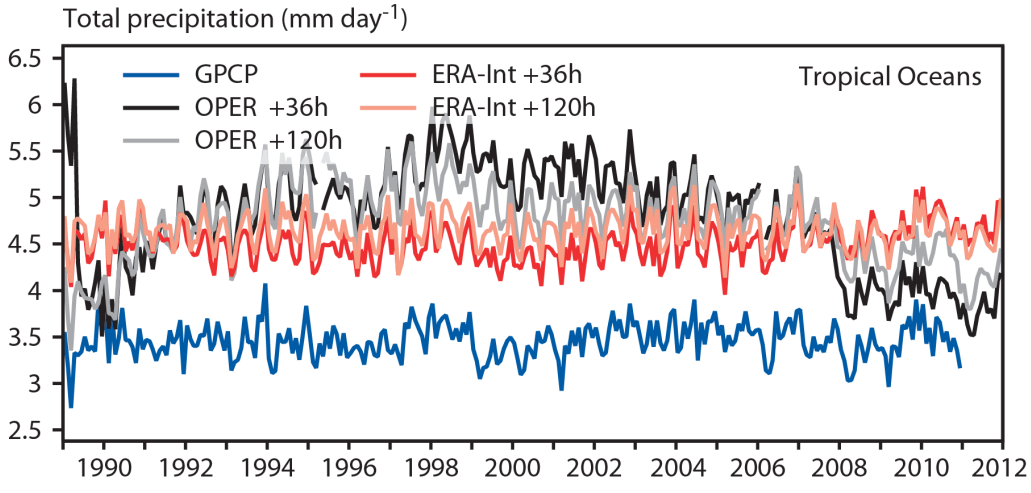

Figure 5. Time series from 1989 to 2012 of precipitation rates (mm day^{-1}) over the tropical oceans from the GPCP2.2 dataset and from ERA-Interim and the operational day+1 and day+5 forecasts

In regions with sufficient and 'accurate' observations, model errors can be quantified by analysis increments which are the corrections the 4D-Var analysis adds to the background forecast, due to information from observations. These increments naturally have a seasonal cycle in the Tropics. As we cannot show them all, we decided to focus on the SON season in 2011 where all the areas with large errors are still apparent. In Figure 6 are depicted seasonal mean values of temperature and wind increments and standard deviations (STDs) of temperature increments. At 1000 hPa the largest wind increments and STDs are along the Inter Tropical Convergence Zone (ITCZ), where the observations, mainly scatterometer data for wind, increase the convergence pointing to a weakening of the Hadley cell during the forecasts. In contrast, at 850 hPa the largest wind increments, mainly stemming from GOES-13 cloud track winds, occur in the East Pacific, whereas the largest STDs of temperature

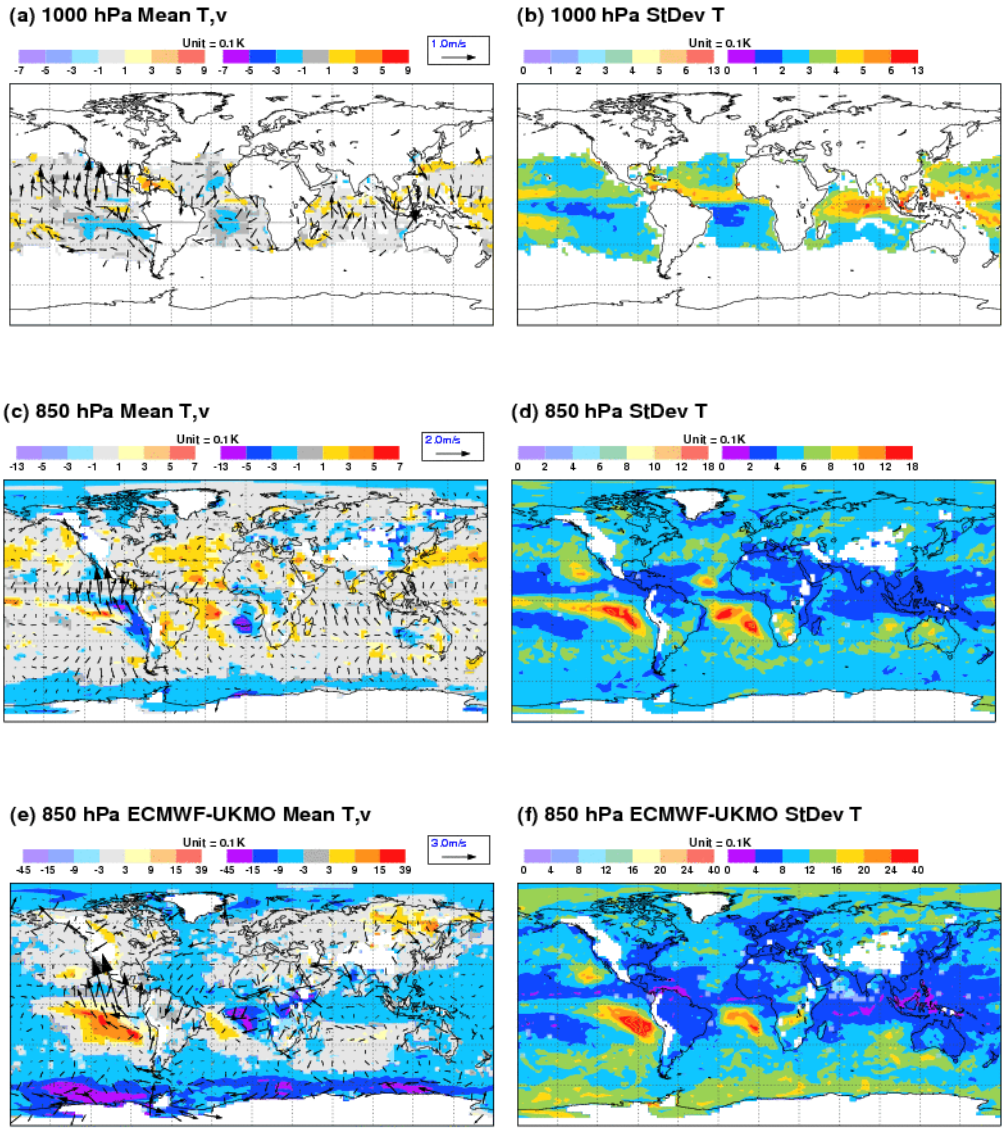

Figure 6. Top two rows: Mean analysis increments (Analysis-Forecast) at 1000 and 850 hPa during OND 2011 for wind (m s^{-1}) and temperature (K) (left column), and standard deviation of temperature (right column). Bottom row is mean analysis difference at 850 hPa ECMWF-UKMO and standard deviation of difference.

occur further west over the trade wind regions. These increments indicate a lack of southerly cross-equatorial flow in the forecasts, and a lack of northerly cross-equatorial flow at 700 hPa (not shown). However, due to the large vertical wind-shear in this region the observation uncertainty from cloud track winds (height assignment), and therefore the analysis uncertainty is also large. To illustrate this further, analysis differences at 850 hPa between ECMWF and the UK Met Office have also been added in Figures 6e-f. The analysis differences are indeed very large in the East Pacific with much stronger cross-equatorial flow in the ECMWF analysis, and similar to Figure 6d the STD of analysis difference for temperature is largest in the trade wind regions.

Finally, day+5 seasonal mean forecast errors of the IFS against own analysis are shown in Figure 7 at 1000 and 850 hPa for both the ensmble mean of the Ensemble Prediction system and the 'deterministic' high-resolution forecasts. The lessons to be learned here are that i) the day+5 forecast errors are very similar to the analysis increments which can be interpreted as the 'error' (note opposite sign convention) of the 6-9 hours background forecast, and that ii) ensemble mean tropical errors are very similiar to the errors of the deterministic forecast as systematic tropical errors occur in the wavenumber 1-3 spectral band (De and Chakraborty, 2004).

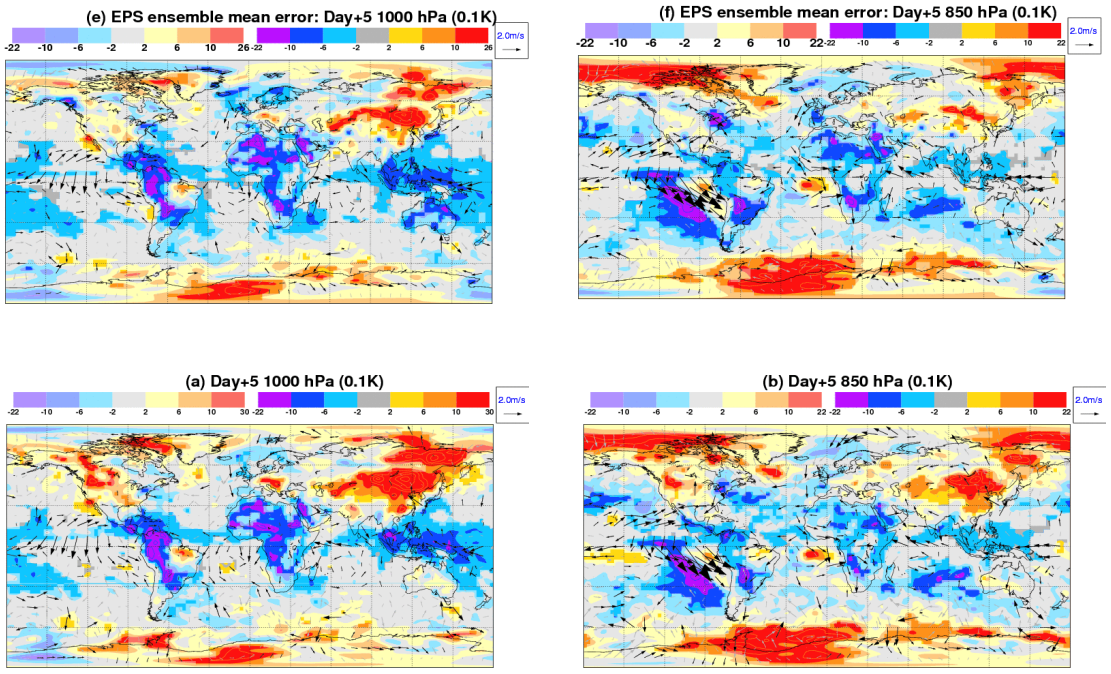

Figure 7. Mean day+5 wind and temperature forecast errors of the IFS (Forecast-Analysis) during SON 2011 from the ensemble mean of the Ensemble Prediction System, top row, and from the high-resolution deterministic forecast, bottom row.

5 Seasonal forecasts

An accurate model climate is fundamental for accurate seasonal forecasts including intraseasonal variability. The convection is an important player but its performance is dependent on other model aspects like the radiation and the land-surface scheme. Here the climate of the IFS for the latest cycle 38r1 (operational from June 2012) is evaluated over a period of 30 years based on a 3-member ensemble of uncoupled seasonal 7-months integrations at resolution T255 (Magnusson, 2012). For specific applications the evaluation is also based on longer integrations covering either one or up to 10 annual cycles.

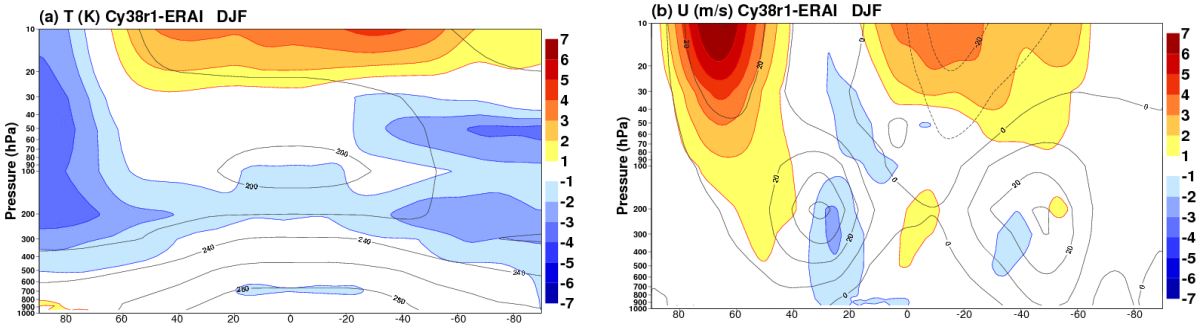

Figure 8. Zonal mean temperature and u-wind differences during DJF between seasonal forecasts (30-year average) and the ERA-Interim.

As shown in Figure 8, the zonal mean bias for temperature and zonal wind against the ERA-Interim amount to around 0.5 K, and 1-2 m s^{-1}, respectively. These biases are also characteristic for the day+5 mean forecast errors (Figure 7), and are already apparent through the day+1 total forecast tendency imbalance (Figure 1). Concerning the comparison of surface fields with observations the two errors that stand out are an overestimation of the Asian summer monsoon rainfall (Figure 9a) and a shortwave radiation bias over the tropical and subtropical oceans (Figure 9b). There is a strong overestimation of West Indian rainfall, and of the South-East Asian Monsoon in general that consequently also leads to too strong tropical easterlies at the Equator (and in coupled mode to too cold near-Equator sea-surface temperatures (SSTs)). The reasons for the overestimated diabatic heating are not yet entirely clear, but studies (see MJO Section) indicate that the lower to mid-tropospheric convective moistening is slightly overestimated. However, other processes notably errors in the aerosol climatology also play a role as indicated by sensitivity studies. The shortwave radiation biases of O(- 10-20) W m^{-2} in the tropical and subtropical cumulus and trade-cumulus regimes, and of O(+40) W m^{-2} in the stratocumulus areas (Figure 9b) have already been investigated by Ahlgrimm and Köhler (2010). The authors showed that in general stratocumulus cloud amount is underestimated whereas the water content in the trade-cumuli is too high producing clouds that are too reflective. A solution to this problem could be obtained by reducing the shallow convection activity, via reducing the mass fluxes, but this would impact the vertical stability and therefore the rainfall and the overall model performance. To conclude this section two more aspects of

tropical convection are discussed, namely the responsiveness to the SSTs, and the diurnal cycle of convection.

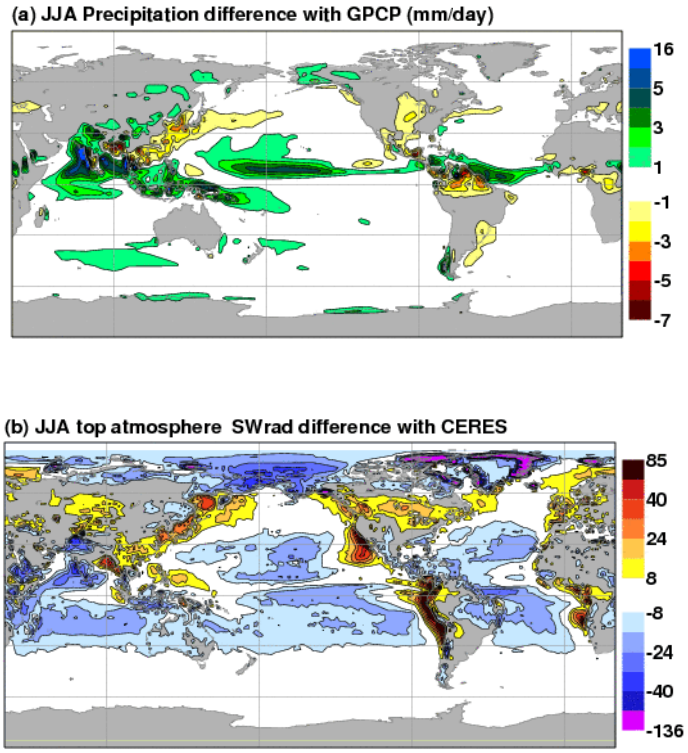

Figure 9. JJA model precipitation differences (mm day^{-1}) against GPCP2.2, and net SW radiation differences (W m^{-2}) at the top of the atmosphere against CERES.

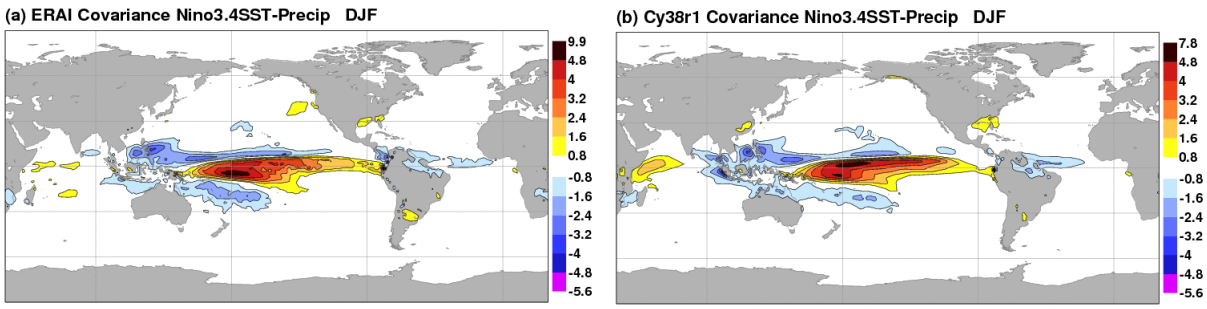

Figure 10. Covariance during DJF between average SSTs in the Nino3.4 area (central equatorial Pacific) and precipitation from the ERA-Interim (a) and the IFS seasonal forecasts (b).

The covariances between the SSTs in the Nino3.4 area (central equatorial Pacific) and the preci-pitation have been computed in Figure 10 from the ERA-Interim and from the seasonal forecasts. In general the model reproduces the 'observed' covariances where positive SST anomalies project on the troposphere through convection producing more rainfall, and suppress convection in the West Pacific and on either side of the Equator. Models tend to reproduce these covariances when the SST gradients are large but tend to have difficulties in correctly placing the precipitation when the SST gradients are small as e.g. in the equatorial Indian Ocean (Williamson et al. 2012).

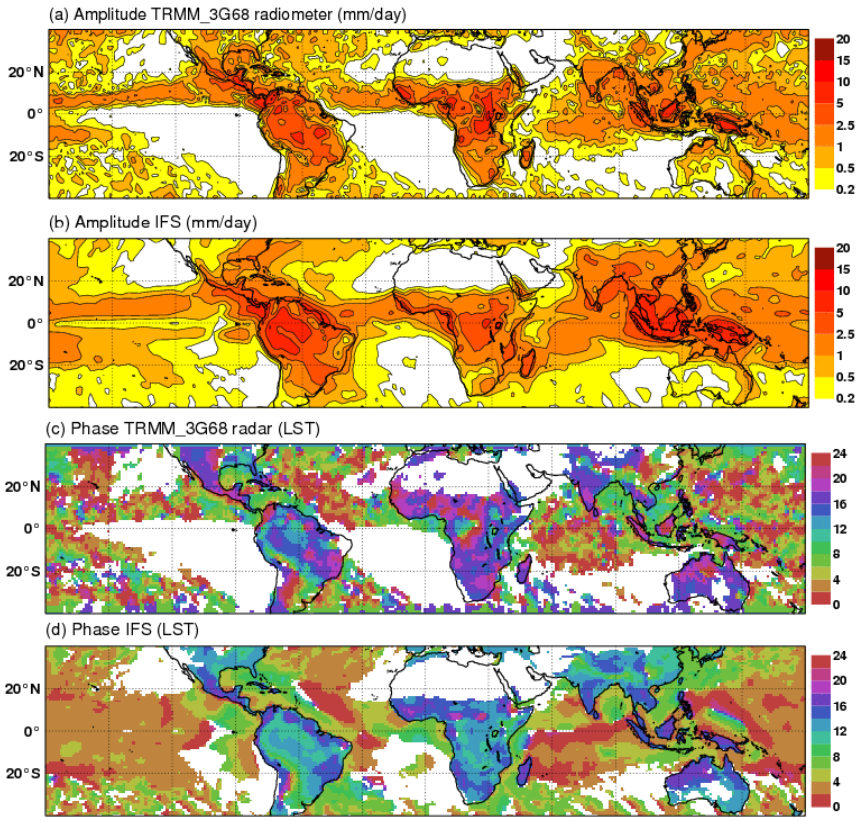

Figure 11. Amplitude (mm day-1,) , (a)-(b), and phase (LST), (c)-(d), of the diurnal cycle of precipitation as obtained from the first harmonics of a 10-year 1-hourly TRMM climatology and an ensemble of 1-year integrations at T159.

Finally, the diurnal cycle of convection is evaluated in Figure 11 by computing the first harmonic (amplitude and phase) from the observed precipitation (a 1-hourly climatology derived from TRMM by Y. Takayabu and colleagues) and the seasonal forecasts. Concerning the amplitude, model and observations (TRMM radiometer) are in good agreement, producing maximum amplitudes of up to 15 mm day^{-1} over tropical land. Maximum rainfall rates in the observations (TRMM radar) over land occur during late afternoon and early evening, whereas over the oceans maximum rainfall occurs during the early morning hours. The model reproduces the overall spatial variations in the phase of the rainfall, but over land the model rainfall precedes the observations by 3-4 hours. As discussed e.g. in Slingo et al. (1992) this is a problem common to many models. Due to the complexity of the processes involved we do not yet see, in spite of many trials, a robust solution to this when using a convection parametrization scheme, while it has been demonstrated that high-resolution explicit simulations of deep convection with horizontal resolutions <1 km can realistically reproduce the diurnal cycle over land. However, we do not think that the phase error in the diurnal cycle over land is a major limit for seasonal forecasting (e.g. for the prediction of tropical waves and the MJO, maybe apart from African easterly waves) as from a dynamical point of view the most important is to reproduce the amplitude and overall amount of convection.

6 The MJO

Realistic predictions of the MJO are essential for realistic tropical seasonal forecasts, and through their teleconnections are also key to meaningful seasonal forecasts in the middle latitudes (Vitart and Molteni, 2009). Particular attention has been given to the MJO during the Year of Tropical Convection (YOTC), defined as the period from 2008 to March 2010 (Walliser et al. 2012), where ECMWF made available to the scientific community the entire high-resolution forecasts including process budgets. Also the DYNAMO campaign during the autumn/winter 2011/12 season has been dedicated to the study of MJO initiation over the Indian Ocean. A major MJO event during that campaign during end of November 2011 is illustrated in Figure 12 including the IR satellite image and ECMWF analysed winds at 850 and 200 hPa. One notices, quite similar to a Kelvin wave structure, the low-level westerly wind burst in the western part of the convective clusters and easterly inflow to the east. However, differing from the Kelvin wave structure discussed in Section 2 (v-component=0) there are low-level cyclonic Rossby gyres, that often give birth to tropical cyclones, und upper-level anticyclonic gyres that connect with the subtropical jet streams.

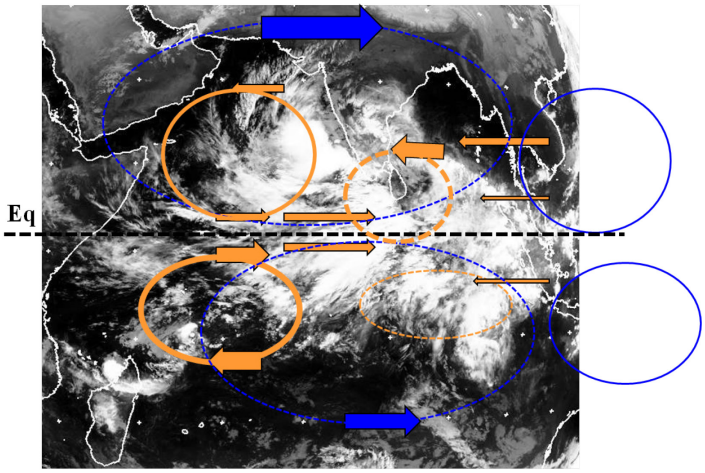

Figure 12. Meteosat IR satellite image from 27 November 2011 00 UTC with simplified ECMWF analysis of an MJO event over the Indian Ocean: 850 hPa wind field (orange), 200 hPa winds (blue).

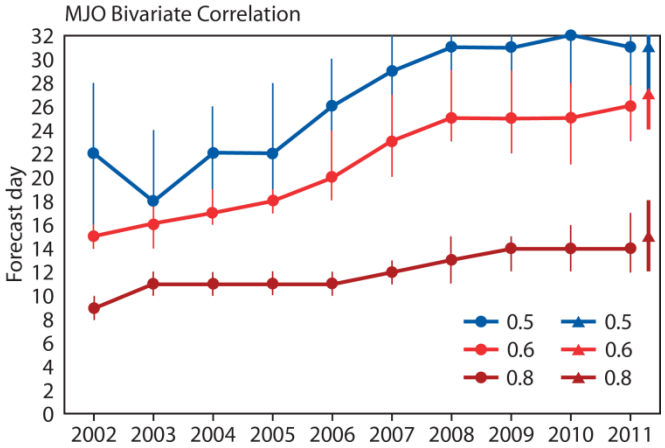

Figure 13. Evolution of skill of MJO forecasts based on hindcasts with model cycles between 2001 and 2012. The skill measure is the correlation with analysed OLR and 850 and 250 hPa winds.

The evolution of the skill of our MJO forecasts during the last decade is depicted in Figure 13. Considering a meaningful correlation of 0.6 the predictability of the MJO has evolved from 15 days in 2002 to 26 days in 2012, with a particular strong increase in 2007/2008 due to model physics, notably the convection. However, the current predictability limit is still far from the theoretical predictability limit which is about 45 days or one cycle. In the following we make use during YOTC of the available forecasts/analysis, namely the operational system, and the ERA-Interim. We also produced a set of reforecasts using the operational cycle but with the convection scheme reverted back to the version before 2008 to assess which model features contributed to the important predictability improvements in recent years.

Following Wheeler and Hendon (2004) it is convenient to composite the MJO in different phases, and here we focus on the phases 2/3, when the MJO is over the Indian Ocean, and 6/7 when it is over the West Pacific. The differences in model tendencies between phases 6/7-2/3 are shown in Figure 14, note that the true sign of the tendencies corresponds to phase 6/7 so the longitude range from 120-180° East. On notices that the MJO is determined to first order by a balance between a deep dynamic cooling mode and a deep convective heating mode, but the stratiform heating/cooling dipole is also important as is the radiation, and in particular over the Indian Ocean. It is this latter region which is the most sensitive region for the MJO and modifications to either of the model processes will alter the MJO predictions. Next we focus on the relation between convection and moisture for the different model versions. Following Hirons et al. (2012) are compared in Figure 15a against the TRMM observations the pdfs of 24-hour rain rates in the 0-30 mm day^{-1} bins of the operational model, the ERA-Interim and the forecasts labeled 'CONV' with the convection reverted to the version before 2008,. The operational forecasts raesonably follow the observations but still overstimate the rainfall. However, the ERA-Interim heavily overestimates the precipitation in the 4-15 mm day^{-1} rain bins. The CONV experiment shows that the improvements since the ERA-Interim mainly stem from the convection. Furthermore, an overestimation of rainfall in the 4-15 mm day^{-1} is or has been common to several global models, in particular those that use a convection scheme with very low

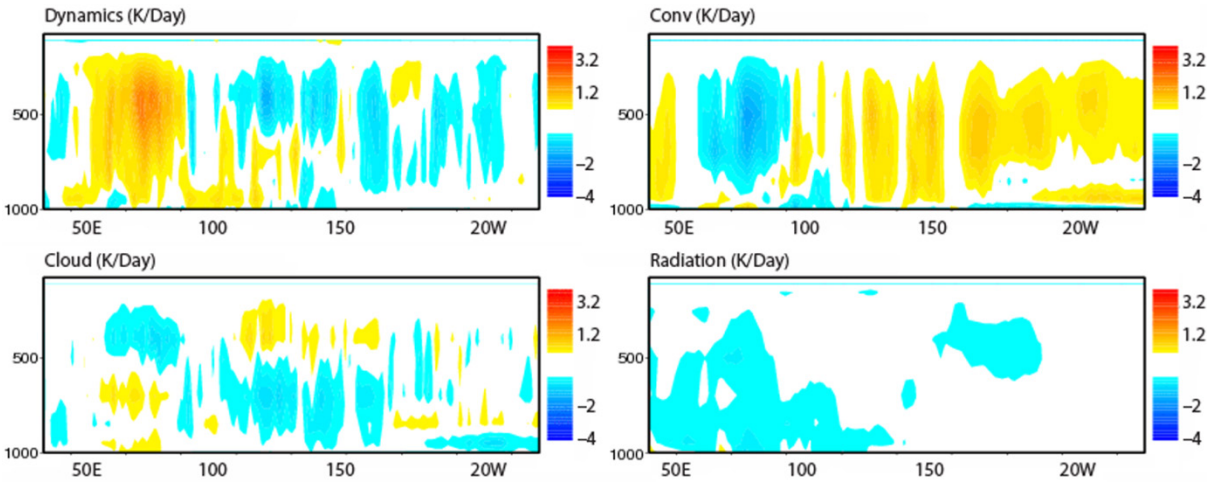

Figure 14. Composite of day+1 model tendencies plotted as the difference between the phases 6/7 (West Pacific) and 2/3 (Indian Ocean) of the MJO.

entrainment rate, and therefore little sensitivity to tropospheric moisture variations. This is also demonstrated in Figure 15b where the rainfall rate is plotted as a function of the total column water content (TCW) -the functional relation is obtained from a 2D pdf and summing over the columns of the matrix. Indeed, whereas the ERA-Interim and CONV produce precipitation already for TCW of 35 kg m^{-2}, the operational version suppresses convection until a TCW value of 50 kg m^{-2} due to a strong entrainment.

a) b)

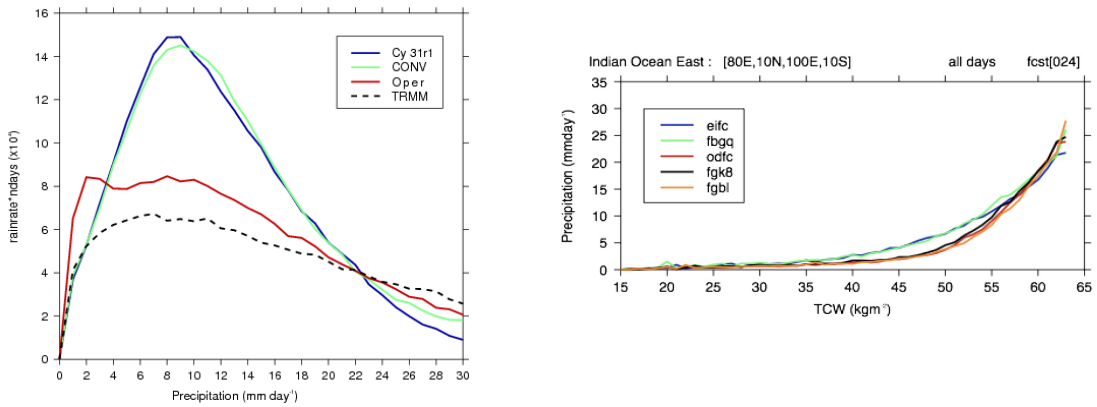

Figure 15. (a) Pdf of rain rates for the ERA-Interim, CONV, the operations and from TRMM radar. (b) Precipitation as function of total column water vapor, same experiments as (a).

The 'permanent' convective activity (heating) in CONV and ERA-Interim results in a significant weakening of the MJO amplitude by day+5-10 (not shown). The reasons for this are multiple: the troposphere cannot recharge with moisture, the horizontal pressure gradient cannot be maintained, and the energy conversion in the upper-troposphere is not realistic as it might occur in the wrong phase of the upper-level temperature or vertical velocity anomaly. We try to illustrate some of these effects in the last two Figures 16 and 17 that focus on a single MJO event during March/April 2009.

The moisture anomaly during the passage of an MJO over the Indian Ocean is shown in Figure 16 as obtained from concatenated day+1 and day+5 forecasts. Before and after the MJO event (positive OLR anomaly) the middle and upper troposphere is dry (mainly due to subsidence), while around 5 to 10 days before the peak of the MJO there is strong moistening between 900 and 600 hPa that continues during the onset of the MJO (mainly due to dynamical lifting). Figure 16 also demonstrates that the humidity anomaly is larger in the day+5 forecasts, reflecting the overall moistening tendency (bias) in the IFS discussed previously. If we now repeat the excercise but plotting instead of the moisture anomaly the difference in total physics tendencies between OPER and CONV (Figure 17) then one recongizes that the suppresion of convection in OPER results at day+1 in an overall relative mid-tropospheric cooling/moistening tendency with respect to CONV which clearly results at day+5 in a stronger convective heating/drying tendency during the MJO event between 5 and 15 April, and therefore a stronger amplitude of the MJO.

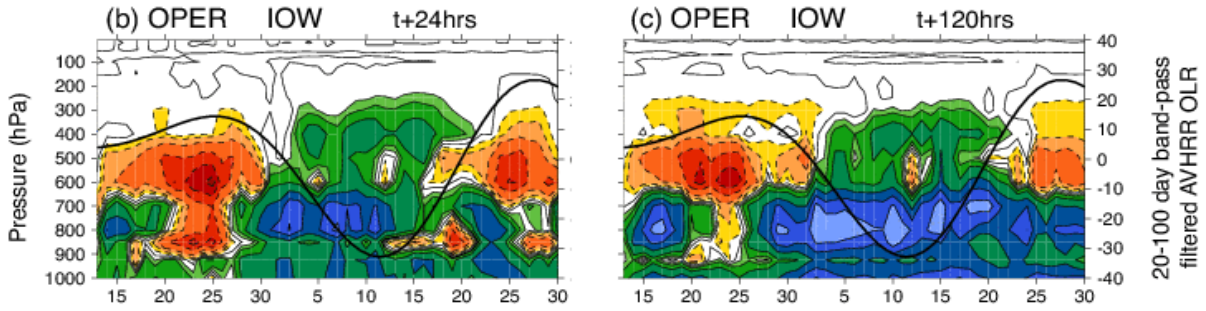

Figure 16. Time-vertical cross section over the equatorial Indian Ocean during March-April 2009 of moisture differences with respect to the initial condition from concatenated daily day+1 and day+5 forecasts. The black line shows the OLR anomaly with the MJO event peaking between 10-15 April.

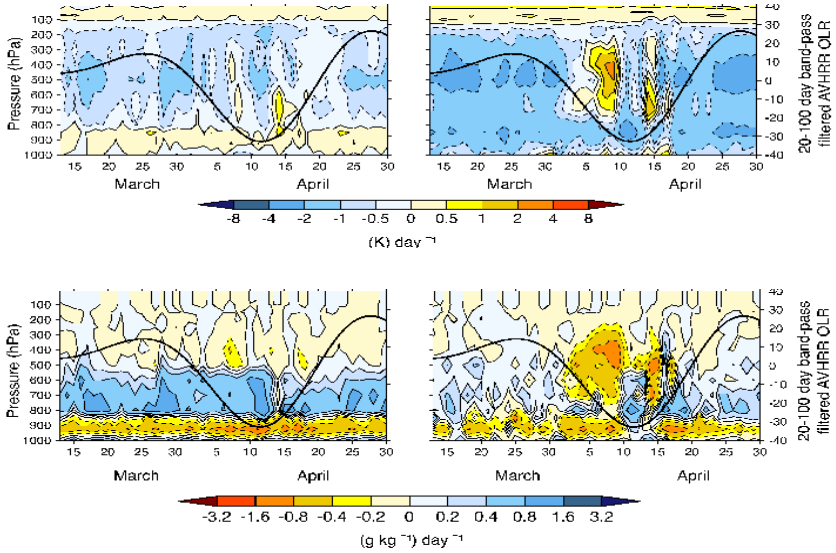

Figure 17. As Figure 16, but for the difference in total physics tendencies for temperature and specific humidity at day+1 and day+5 between OPER and CONV.

7 Summary and Perspectives

The main messages from this tropical convection overview can be summarized as follows:

- The most important area for energy generation and conversion is the upper-tropical troposphere. This is the dynamical mode.
- Convective heating must occur in the right phase of the large-scale wave, and as temperature variations are small, the convection (parameterization) must show the right sensitivity to mid-tropospheric moisture. This is also the moisture mode interpretation of the MJO where moistening ahead of the MJO occurs by advection and lifting and through shallow and congestus clouds, and where the drying occurs by deep convection during the active phase.
- The main forecast errors concern a spindown of the Hadley cell (why?), and a too strong South-East Asian Monsoon which is also related to a moistening tendency in the model in connection with an easterly wind bias.
- The largest analysis uncertainty and largest 950-700 hPa wind errors concern the East tropical Pacific. The systematic tropical errors differ little between the

high-resolution system and the ensemble mean of the Ensemble Prediction System.

Concerning areas for progress in the coming years, we think that the largest potential is for further improvements in the MJO prediction. Also we hope to improve the Asian Monsoon heating, possibly through a reduction of the moistening tendency by reducing the shallow convective activity. However, substantially improving the phase error in the diurnal cycle over land will be difficult to achieve with a simple convection parameterization, and one might need to wait for the convection permitting systems to become operational. Finally, and to our surprise it appears that there is also a large forecast uncertainty in the clear sky radiative forcing through uncertainties in aerosol optical depth and optical properties. Preliminary experiments with new aerosol initial fields derived from the MACC project (Figure 18) indicate very large radiative flux divergence differences of 10-40 W m^{-2} (Figure 18a), notably over the Horn of Africa, compared to operations that use the Tegen aerosol climatology. The resulting difference in the precipitation field is large with values attaining 10 mm day^{-1} over West India, suggesting that a new more realistic aerosol climatology could potentially improve longstanding monsoon errors in this region.

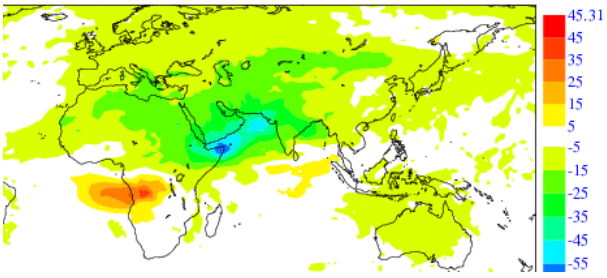

Figure 18 a Difference in total radiative flux divergence (W m^{-2}) between forecasts using the MACC derived aerosol optical thicknesses and revised optical properties and the control using the Tegen climatology.

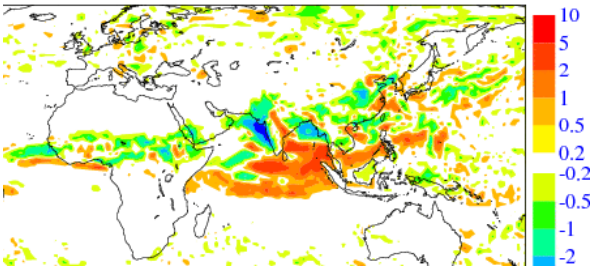

Figure 18b. Same as Figure 17a but for the resulting difference in precipitation rate after day+5.

Acknowledgements

Many colleagues contributed to this work including Peter Bauer, Paul Berrisford, Jean Bidlot, Carla Cardinali, Thomas Haiden, Linda Hirons, Martin Janousek, Daniel Klocke, Linus Magnusson, Jean-Jacques Morcrette, Thony McNally, Fernando Prates, Mark Rodwell, Irina Sandu, Noureddine Semane, and Frédéric Vitart. Our sincere gratitude goes to King-Fai Li from CalTech for providing the wavenumber frequency package, to Yukari Takuyabu from Tokyo University for providing the hourly TRMM climatology dataset, to Nicholas Klingamann from Reading University for providing the NOAA daily OLR data, and to Jörg Trentmann from DWD for providing the climate SAF radiation products. We also warmly thank Sylvie Malardel and Nils Wedi for her help in developing a small planet system (shown only in the presentation), Anton Beljaars, Elias Holm, Lars Isaksen, Erland Källén, Martin Leutbecher and Alan Thorpe for many helpful discussions, and Anabel Bowen Rob Hine, and Els Kooij-Connally for graphical editing.

8 References

Ahlgrimm, M.and M. Köhler, 2010: Evaluation of Trade Cumulus in the ECMWF Model with Observations from CALIPSO. Mon. Wea. Rev., 138, 3071-3083.

Arakawa, A. and W. Schubert, 1974: Interaction of a cumulus ensemble with the large-scale environment. Part I. J. Atmos. Sci., 31, 674-701.

Bechtold, P., M. Köhler, T. Jung, F. Doblas-Reyes, M. Leutbecher, M. Rodwell, F. Vitart and G. Balsamo, 2008: Advances in simulating atmospheric variability with the ECMWF model: From synoptic to decadal time-scales. Q. J. R. Meteor. Soc., 134, 1337-1351.

Bechtold, P., 2012: Atmospheric Moist Convection. ECMWF Lecture Note, available under http://www.ecmwf.int/newsevents/training/lecture_notes/LN_PA.html, 81 pp.

De, S., and D. R. Chakraborty, 2004: Tropical systematic and random error energetics based on NCEP (MRF) analysis-forecast system- A barotropic approach part II: in wavenumber. Proc. Indian Acad. Sci., 113, 167-195.

Hirons, L., P. Inness, F. Vitart and P. Bechtold, 2012: Understanding advances in the simulation of intraseasonal variability in the ECMWF model. Part II: The application of process based diagnostics}, Q. J. R. Meteorol. Soc., revised.

Madden R. A. and P. R. Julian, 1971: Detection of a 40-50 day oscillation in the zonal wind in the tropical Pacific. J. Atmos. Sci., 28, 702-708.

Magnusson, L., M. Alonso-Balmaseda, S. Corti, F. Molteni and T. Stockdale, 2012: Evaluation of forecast strategies for seasonal and decadal forecasts in presence of systematic model errors. ECMWF Technical Memorandum, 676, 30 pp, available from ECMWF, Reading, UK.

Matsuno, T., 1966:.Quasi-geostrophic motions in the equatorial area. J. Meteorol. Soc. Japan, 44, 25-42.

Steinheimer, M., M. Hantel and P. Bechtold, 2008: Convection in Lorenz 92s global cycle with the ECMWF model. Tellus, 60A, 1001-1022.

Simmons, A. J., 1982: The forcing of stationary wave motion by tropical diabatic heating. Q. J. R. Meteorol. Soc., 108, 503-534.

Slingo, J. M., K. Sperber, J.-J. Morcrette, and G. L. Potter, 1992: Analysis of the temporal behavior of convection in the tropics of the European Centre for Medium-range Weather Forecast model}. J. Geophys. Res., 97, 119—135.

Vitart, F. and F. Molteni, 2009: Simulation of the MJO and its teleconnections in an ensemble of 46-day hindcasts. Q. J. R. Meteorol. Soc., 136, 842-856.

Waliser, D. E., M. Moncrieff and many co-authors, 2012: The Year of Tropical Convection: Climate variability and weather highlights. Bull. Americ. Meteorol. Soc., to appear.

Wheeler, M. C. and H. H. Hendon, 2004: An all-seasonal real-time multivariate MJO Index: development of and Index for monitoring and prediction. Mon. Wea. Rev.,132, 1917-1932.

Williamson, D. L., M. Blackburn, and many co-authors, 2012: The Aqua Planet Experiment (APE): Response to changed meridional SST profile. J. Meteorol. Soc. Japan, to appear.

Žagar, N., Andersson, E. and M. Fisher, 2005: Balanced tropical data assimilation based on a study of equatorial waves in ECMWF short-range forecast errors. Q. J. R. Meteorol. Soc., 131, 987-1011.